Enhancement of the dynamic buckling load for a plate by using piezoceramic actuators

R C Batra and T S Geng

Department of Engineering Science and Mechanics, MC 0219, Virginia Polytechnic Institute and State University, Blacksburg, VA 24061, USA

Abstract
We consider geometric and material nonlinearities when studying numerically the transient three-dimensional elastic deformations of a plate with piezoceramic elements perfectly bonded to its top and bottom surfaces, and analyze the effect of the shape and the size of the piezoceramic actuators on increasing the buckling load of the plate. The applied compressive edge load is assumed to increase linearly with time and the plate is taken to have buckled when the maximum transverse deflection at a point equals three times the plate's thickness.

(Some figures in this article are in colour only in the electronic version)

1. Introduction

Whereas in the past material systems and structures were designed based on their passive response to applied loads, recently the construction and operation of space structures have generated an interest in using piezoelectric materials and shape memory alloys (SMAs) to form 'smart' structures. Some of the piezoceramics (PZTs) attached to a structure can be used as sensors and others as actuators to control their deformations and/or to produce a desired response. The SMA actuators can generate actuation strains of 8% when energized by a relatively low energy and the PZT actuators generally require high electric fields to produce noticeable actuation strains. However, the response time of a PZT is in microseconds, and that of SMA actuators is much larger than that of a PZT. Here we investigate the use of PZTs in enhancing the dynamic buckling load of a homogeneous orthotropic elastic plate. The plate's material is modeled as neo-Hookean and that of the PZT by a constitutive relation that expresses the second Piola–Kirchhoff stress tensor as a second degree polynomial in the electric field and the Green–St Venant strain tensor, e.g. see Yang and Batra [1]. Thus the effect of large electric fields applied to the PZT elements can be adequately modeled. The motivation for this is provided by the experimental work of Crawley and Anderson [2] who observed a nonlinear relationship between the applied voltage and the normal strain induced in an unconstrained PZT plate for electric fields exceeding 100 V mm^{-1}. We use the three-dimensional

theory and account for the effect of inertia forces, geometric nonlinearities (nonlinear strain–displacement relations) and material nonlinearities in ascertaining the buckling load of a rectangular plate. The plate is loaded on two opposite edges by axial loads that increase linearly with time while the other two edges are traction free. The problem is analyzed by the finite element method with the computer code developed by Batra and Liang [3].

The flexural rigidity of a plate and hence its buckling load can be passively increased by adding stiffeners to it. However, situations such as esthetics, limited availability of space, packaging requirements, interference with other structural components or weight may restrict the use of stiffeners. In these cases, it may be more beneficial and sometimes absolutely necessary to resort to active methods, such as the one studied here, to enhance the buckling load for the plate.

Previous work on the enhancement of the buckling load of an elastic rectangular plate by using PZT elements includes that of Chandrashekhara and Bhatia [4], Murali Krishna and Mei [5], and Thompson and Griffin [6]. Chandrashekhara and Bhatia [4] used the first-order shear deformation theory, linear kinematics, linear constitutive relations for the PZT and the material of the plate and assumed that the plate buckles when its centroidal transverse deflection equals the plate's thickness. The axial loads applied on two opposite edges of the plate were taken to increase linearly with time. Their numerical results computed for a square thin plate with the length/thickness ratio of 100 showed that the actuation of the PZT elements

increased the buckling load by 4.6%. Murali Krishna and Mei [5] also used the finite element method to analyze the problem but employed the von Karman large deflection plate theory and PZT and PVDF (polyvinylidene fluoride film) actuators. They showed that the voltage to be applied to the PZT elements in order to buckle the plate with all four edges clamped was higher than that required when all edges were simply supported. Thompson and Griffin [6] employed titanium–nickel SMA actuators to control the buckling of a stiffened aluminum plate. They used the commerical code ABAQUS, modeled the structure by plate/shell elements and the actuators by beam elements. The change in the buckling load was found to be almost proportional to the magnitude of the actuation level, and an 8% strain in the SMA actuators enhanced the buckling load by 14%.

Baz and Tempe [7] have designed a closed-loop computer-controlled system employing a titanium–nickel SMA helical spring to increase the buckling load of a long slender beam loaded by an axial compressive load at the rate of $0.0917\,\text{N}\,\text{s}^{-1}$. Thompson and Laughlan [8] experimentally showed that the buckling load of graphite–epoxy strips can be increased from 19.8 to 37.1% by using PZT actuators. DeFaria and deAlmeida [9] employed the von Karman nonlinear strain–displacement relations and linear constitutive relations for both the PZT and beam material. They developed a strategy to exploit the PZT actuation so that the response of a slightly crooked beam is very close to that of a perfect beam. Berlin and Sussman [10] stabilized the first buckling mode through the use of tendons. Meressi and Paden [11] analytically proved that PVDF actuators mounted continuously along the length of a column could be used to stabilize the first mode of the column. Jefferis [12] used an electromagnet to achieve the same goal. Berlin [13] demonstrated the use of induced-strain actuation to control the buckling of a thin steel column and thereby achieved an increase of 5.6 times in the load bearing capacity of the column. Berlin et al [14] have also established the effectiveness of networked arrays of MEMS-based sensors and filamentary PZT actuators to control the buckling instability of a column for loads up to 2.94 times the critical buckling load.

In contrast to the dynamic buckling problem studied here in which the applied axial loads increase linearly with time, other investigators (e.g. see [15]) have considered axial impulses of finite duration applied to the edges of the plate. Typically, the axial velocity or the axial load in the form of a half sine wave is considered. The amplitude and the time period of the sine wave are varied till the plate buckles. The dynamic buckling load is determined by adopting the stability criterion of Budiansky and Hutchinson [16], according to which the structure is unstable if one of the characteristic values associated with its deformations increases rapidly with the amplitude of the applied load. Cui et al [17] determined the deflection of a rectangular elastic–plastic plate loaded by axial loads of fixed duration and defined the buckling load as the one for which the slope of the deflection versus the load curve suddenly increased. These authors also give a brief historical perspective of the dynamic buckling of plates.

Dynamic loads can rarely be represented by a half sine wave or a half rectangular wave of short duration; they usually increase suddenly and then slowly die out. Here we assume that the applied load increases linearly with time and the plate buckles during the time the load is increasing.
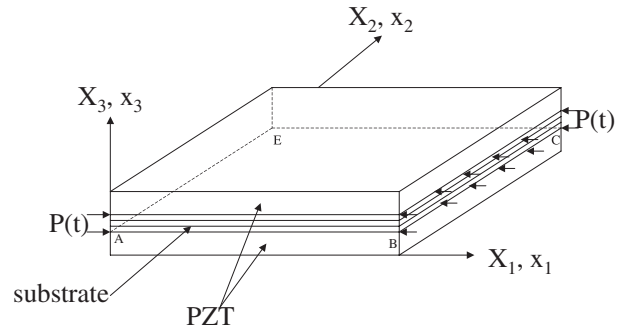

Figure 1. Schematic sketch of the problem studied.

Results presented herein show that PZT elements bonded to the top and the bottom surfaces of a rectangular plate when suitably activated can enhance the buckling load of a graphite–epoxy plate by 58.5%.

2. Formulation of the problem

We use rectangular Cartesian coordinates to describe the transient electromechanical finite deformations of a system consisting of a plate with PZT elements perfectly bonded to its top and bottom surfaces; a schematic sketch of the problem studied is shown in figure 1. In the referential description of motion, and in the absence of body forces and distributed charges, equations governing these deformations are

$$T_{iL,L} = \rho_0 \ddot{u}_M \delta_{iM}, \qquad i = 1, 2, 3; \quad L = 1, 2, 3 \quad (1)$$

$$D_{L,L} = 0. \quad (2)$$

Here T_{iL} is the first Piola–Kirchhoff stress tensor, sometimes also called the nominal or the engineering stress tensor, ρ_0 is the mass density in the reference configuration, u_M is the displacement of a point, D_L is the electric displacement, a superimposed dot indicates the material time derivative, δ_{iL} is the Kronecker delta, and a comma followed by an index L signifies partial differentiation with respect to the position X_L occupied by a material point in the reference configuration. A repeated index implies summation over the range of the index. The lower and upper case indices denote the component of a tensor with respect to coordinates in the present and the reference configurations, respectively. Equation (1) expresses the balance of linear momentum in the absence of body forces, and equation (2) the balance of electric charges when there are no distributed charges present. However, as is usually done, the inertia term associated with the balance of electric charge has been neglected. Because we have used the referential description of motion, the equation expressing the balance of mass is not needed to find the displacements of a point; it will be required if the present mass density is to be determined.

Balance laws (1) and (2) are to be supplemented by constitutive relations. The material of the plate is assumed to be homogeneous and orthotropic and is modeled as neo-Hookean. That is

$$S_{LM} = C_{LMPQ} E_{PQ} \quad (3)$$

where S is the second Piola–Kirchhoff stress tensor, E the Green–St Venant strain tensor, and C the fourth-order

elasticity tensor with nine independent components for an orthotropic material. Since $S_{LM} = S_{ML}$ and $E_{PQ} = E_{QP}$, each can be expressed as a six-dimensional vector. In this notation, C will be a 6×6 symmetric matrix. Batra [18] has compared the response predicted by four linear constitutive relations such as equation (3) for finite deformations of isotropic elastic materials. He showed that the analog of constitutive relation (3) for isotropic materials predicts a stiffening behavior. That is, in simple extensional and shearing deformations, the tangent modulus increases with an increase in a measure of the deformation. For the problems studied herein, this stiffening of the material is negligible because the maximum strain induced in the structure is less than 11%. The PZT is modeled as a homogeneous transversely isotropic material with the axis of transverse isotropy along the unit vector a. We anticipate applying large electric fields W to it along the direction a. Thus we incorporate second-order terms in E and W in its constitutive relation. Yang and Batra [1] have derived the following second-order constitutive relations for a PZT that is stress free in the reference configuration:

$$
\begin{aligned}
S = {} & (2c_1 I_1 + c_3 I_2 + e_1 I_3 + 3\lambda_1 I_1^2 + 2\lambda_3 I_1 I_2 + \lambda_4 I_2^2 \\
& + \lambda_5 II_1 + \lambda_7 II_2 + 2\nu_1 I_1 I_3 + \nu_2 I_3^2 + \nu_7 II_3 + \nu_9 II_4 \\
& + \nu_{14} I_2 I_3) a \otimes a + (2c_2 I_2 + c_3 I_1 + e_2 I_3 + 3\lambda_2 I_2^2 + \lambda_3 I_1^2 \\
& + 2\lambda_4 I_1 I_2 + \lambda_6 II_1 + \lambda_8 II_2 + 2\nu_2 I_2 I_3 + \nu_4 I_3^2 + \nu_8 II_3 \\
& + \nu_{10} II_4 + \nu_{14} I_1 I_3) \mathbf{1} + (c_4 + \lambda_5 I_1 + \lambda_6 I_2 + \nu_5 I_3) \\
& (a \otimes E \cdot a + a \cdot E \otimes a) \\
& + 2(c_5 + \lambda_7 I_1 + \lambda_8 I_2 + \nu_8 I_3) E + (e_3 + \nu_9 I_1 + \nu_{10} I_2 \\
& + \nu_{11} I_3)(a \otimes W + W \otimes a) \\
& + 3\lambda_9 E^2 + \nu_{12} W \otimes W + \nu_{13}(a \otimes E \cdot W + W \cdot E \otimes a \\
& + W \otimes E \cdot a + a \cdot E \otimes W) \\
-\pi = {} & (2\epsilon_1 I_3 + e_1 I_1 + e_2 I_2 + 3\mu_1 I_3^2 + \mu_2 II_3 + \nu_1 I_1^2 \\
& + 2\nu_2 I_3 I_1 + \nu_3 I_2^2 + 2\nu_4 I_3 I_2 \\
& + \nu_5 II_1 + \nu_6 II_2 + \nu_{11} II_4 + \nu_{14} I_1 I_2) a \\
& + 2(\epsilon_2 + \mu_2 I_3 + \nu_7 I_1 + \nu_8 I_2) W \\
& + 2(e_3 + \nu_9 I_1 + \nu_{10} I_2 + \nu_{11} I_3) E \cdot a \\
& + 2\nu_{12} E \cdot W + 2\nu_{13} E^2 \cdot a,
\end{aligned}
$$
(4)

where

$$
I_1 = a \cdot Ea, \qquad I_2 = \operatorname{tr} E, \qquad I_3 = a \cdot W
$$

$$
II_1 = a \cdot E^2 a \qquad II_2 = \operatorname{tr} E^2 \qquad II_3 = W \cdot W
$$
(5)

$$
II_4 = a \cdot EW + W \cdot Ea.
$$

Here π is the polarization vector that is related to the electric displacement D, the electric field W and the electric potential ϕ through

$$
\pi_L = D_L - \varepsilon_0 J X_{L,i} X_{K,i} W_K, \quad W_K = -\phi_{,K}
$$
(6)

where ε_0 is the permittivity of the free space, $J = \det(x_{i,K})$, x is the present position of the material point that occupied place X in the reference configuration, and a comma followed by index i denotes partial differentiation with respect to x_i. Furthermore, in equations (4) and (5), $\mathbf{1}$ is the identity tensor, $c_1, \ldots, c_5$, $\lambda_1, \ldots, \lambda_8$, $\nu_1, \ldots, \nu_{14}$, e_1, e_2, e_3, μ_1 and μ_2 are material constants, $a \cdot b$ denotes the inner product between vectors a and b, and the tensor product, $a \otimes b$, between them

is defined as $(a \otimes b)c = (b \cdot c)a$ for every vector c. The neo-Hookean relation for the PZT is obtained from equations (4) and (5) by keeping terms linear in E and W. We note that Batra and Yang [19] have derived second-order constitutive relations for porous PZT materials.

Tensors S and T are related to each other through

$$
T_{iK} = x_{i,L} S_{KL}
$$
(7)

and to the Cauchy or the true stress tensor σ by

$$
\sigma_{ij} = J^{-1} x_{i,L} x_{j,M} S_{LM}.
$$
(8)

The Green–St Venant strain tensor, E, is expressed in terms of the mechanical displacements $u = x - X$ as follows:

$$
E_{KL} = (u_{K,L} + u_{L,K} + u_{M,K} u_{M,L})/2.
$$
(9)

We note that the classical infinitesimal theory follows from equations (1)–(9) by neglecting in them the contributions from the second-order terms in $u_{M,K}$ and W_K. In the linear theory, the three stress tensors S, T and σ coincide with each other.

The perfect bonding condition at the common interface Γ_{int} between the PZT and the plate can be stated as

$$
[u_K] = 0, \qquad [T_{iL}] N_L = 0 \qquad [\phi] = 0
$$

$$
[D_L] N_L = 0 \qquad \text{at} \quad \Gamma_{int}
$$
(10)

where N is a unit normal to Γ_{int}, and $[f]$ denotes the jump in the values of f across the interface. Equations (10) imply that the mechanical displacements, surface tractions, the electric potential and the normal component of the electric displacement are continuous across the common interface Γ_{int}.

The plate and the PZT particles are assumed to be initially at rest and stress free in the reference configuration. Thus initial displacements and velocities of all material particles are zero. With reference to the schematic sketch and the coordinate axes depicted in figure 1, we apply the following boundary conditions:

$T_{i1} = -p(t)\delta_{i1}$	on plate surfaces $X_1 = 0, L_1$
$T_{i2} = 0$	on plate surfaces $X_2 = 0, L_2$
$u_3 = 0$	at points on lines AB, BC, CE
	and EA of the plate
$D_L N_L = 0$	on the plate and PZT surfaces $X_1 = 0$,
	L_1, and $X_2 = 0, L_2$ (11)
$\phi = 0$	on the PZT surfaces bonded to the plate
$\phi = \phi_a$	on the top surface of
	the upper PZT layer
$\phi = \phi_b$	on the bottom surface of
	the lower PZT layer.

That is, the square plate is supported on edges AB, BC, CE and EA, and is loaded on the two opposite surfaces by in-plane time-dependent axial compressive loads with the other two surfaces of the plate free of in-plane tractions. The surfaces of the plate bonded to the PZTs are electroded with electrodes of negligible thickness. All surfaces, except where electric potentials are prescribed, are electrically insulated. Note that, at points on lines AB and CE, the displacement in the X_3 direction and surface tractions in the X_1 and X_2 directions vanish. At points on lines BC and EA, the displacement in the X_3 direction and surface tractions in the X_2 direction vanish.

3. Numerical solution and discussion of results

The aforementioned problem is solved numerically by using the finite element method. The domain occupied by the plate and the PZT layers is divided into the union of disjoint eight-node brick elements. Following the procedure used to derive the Galerkin formulation of the problem, e.g. see [20], we obtain from equations (1) and (2) the following set of coupled nonlinear ordinary differential–algebraic equations:

$$M\ddot{d} = F^{\text{ext}}(t) - F^{\text{int}}(d(t), \phi(t)) \tag{12a}$$

$$P_{\text{int}}(d(t), \phi(t)) = P_{\text{ext}}(t). \tag{12b}$$

Here M is the mass matrix, d the vector of nodal mechanical displacements in both the plate and the PZT layers, ϕ the vector of nodal electric potentials in PZT elements only, F^{ext} and F^{int} are vectors of nodal forces equivalent respectively to externally applied surface tractions and internal stresses and electric fields developed in the body at time t, P_{int} is the nodal charge vector equivalent to the internal polarization in PZT elements, and P_{ext} is the externally applied nodal charge vector. A finite element code based on equations (12) has been developed and validated by Batra and Liang [3]. It uses the $2 \times 2 \times 2$ integration rule to evaluate the element mass matrix and the element load vectors. The mass matrix is lumped by using the row-sum technique. Equation (12a) is solved by the central-difference method which is explicit, conditionally stable and, for linear one-dimensional problems, gives exact time periods for the waves. After every time step, the nonlinear equations (12a) are discretized and we set

$$\Delta t = 1.8/\omega_{\max}. \tag{13}$$

The maximum frequency, $\omega_{\max}$, of the discretized structure is computed after every time step. Within each time step, the nonlinear algebraic equations (12b) are solved by the Newton–Raphson iterative method.

Recalling that the size of the time step varies as the solution evolves, we used the following relation (14) to compute nodal displacements at time t_{n+1} from a knowledge of their values at time t_n:

$$d(t_{n+1}) = \Delta t_2 M^{-1} \left[(F^{\text{ext}}(t_{n+1}) - F^{\text{int}}(t_{n-1})) \frac{\Delta t_1 + \Delta t_2}{2} \right.$$
$$\left. + \left(\frac{1}{\Delta t_1} + \frac{1}{\Delta t_2} \right) d(t_n) + \frac{d(t_{n-1})}{\Delta t_1} \right]. \tag{14}$$

Here $\Delta t_1 = t_n - t_{n-1}$ and $\Delta t_2 = t_{n+1} - t_n$. Values of $d(-\Delta t_1)$ are found from those of $d(0)$, $\dot{d}(0)$ and $\ddot{d}(0)$ by using a one-step method with $\ddot{d}(0)$ computed from equation (12a). We used Batra and Liang's [3] finite element code to study the buckling problem.

3.1. Buckling of a column

In an attempt to delineate the difference in the buckling loads under quasistatic and dynamic deformations, and to establish our methodology of determining the buckling load in transient deformations, we first study the problem for a slender column. The 40 mm × 1 mm × 1 mm steel column modeled as an isotropic material with Young's modulus $E = 200$ GPa, the shear modulus $G = 79$ GPa, and the mass density $\rho =$

Table 1. Dependence of the buckling load for a pinned–pinned column upon the loading rate.

Loading rate (kN s⁻¹)	Buckling load (N)	Dynamic load amplification factor (DLAF)
1000	220.8	8.59
200	89.6	3.49
100	66.6	2.59
20	43.4	1.69

7860 kg m⁻³ is loaded only on the top and bottom surfaces by equal and opposite axial compressive tractions that increase linearly with time t. The column was divided into 40 uniform cubic elements along its length. The initial shape of the column was taken to be a half sine wave with amplitude equal to 1% of the thickness of the column. The axial load applied at the ends of the column was assumed to increase linearly with time t. The Euler buckling load for static deformations of the steel column is 25.7 N. For the dynamic problem, the column was assumed to buckle when the lateral deflection at the midspan equaled three times the width of the column, or 3 mm for the problem being studied. As shown below in table 1, the buckling load computed according to this criterion was found to strongly depend upon the rate of rise of the axial load.

The DLAF [21] equals the buckling load under dynamic loading divided by the Euler buckling load under quasistatic conditions. The computed results clearly indicate that the DLAF decreases with a decrease in the rate of loading. In order to assess the effect of inertia forces on the DLAF, we artifically reduced the mass density of the column's material to 786 kg m⁻³, i.e. to 10% of its true value. In this case, loading rates of 10^6, 2×10^5, 10^5 and 2×10^4 N s⁻¹ resulted in DLAFs of 4.42, 2.21, 1.84 and 1.56, respectively. Thus the DLAF decreases monotonically as the effect of inertia forces is diminished, and our criterion to ascertain the dynamic buckling load is reasonable. Because of the geometric nonlinearities considered, the buckling load for quasistatic loading need not equal the Euler buckling load.

3.2. Buckling of an orthotropic plate

In the second example problem, a square graphite–epoxy plate of side 10 mm and thickness 0.25 mm with fibers oriented parallel to the X_1 axis was divided into $20 \times 20 \times 2$ uniform elements. The values of nonvanishing elastic moduli are

$C_{1111} = 152.35$ GPa, $\qquad C_{2222} = C_{3333} = 9.99$ GPa

$C_{2323} = C_{1313} = 7.1$ GPa $\qquad C_{1122} = C_{1133} = 3.92$ GPa

$C_{2233} = 3.07$ GPa, $\qquad C_{1212} = 2.5$ GPa

and the mass density, ρ, equaled 1600 kg m⁻³. For infinitesimal deformations, these correspond to

$E_1 = 150$ GPa, $\qquad E_2 = E_3 = 9$ GPa

$\tilde{\nu}_{12} = \tilde{\nu}_{23} = \tilde{\nu}_{13} = 0.3 \qquad G_{12} = G_{31} = 7.1$ GPa

$G_{23} = 2.5$ GPa.

Here E_1 equals Young's modulus in the direction of the fibers, E_2, E_3 are Young's moduli in the transverse directions, G_{12}, G_{23}, G_{31} are shear moduli and $\tilde{\nu}_{12}$, $\tilde{\nu}_{23}$, $\tilde{\nu}_{13}$ are Poisson's ratios. For the simply supported plate loaded only

on the surfaces $X_1 = 0$, 10 mm by uniformly distributed axial compressive forces along the X_1 direction, the linear elasticity theory gives a buckling load of 23 064 N m^{-1}, e.g. see [22]. In the numerical solution of the problem by the finite element method, the initial shape of the midsurface of the plate in the X_1 and X_2 directions was taken to be a half sinusoidal curve with an amplitude equal to 0.33% of the plate's thickness. The plate was assumed to have buckled when the transverse displacement (i.e. the displacement in the X_3 direction) equaled three times its thickness. For loading rates of 3.2×10^7 and 1.6×10^7 N m^{-1} s^{-1}, the buckling loads were found to be 38 500 and 32 400 N m^{-1}, respectively, which resulted in DLAFs of 1.67 and 1.41.

3.3. Enhancement of the dynamic buckling load for a plate with PZT elements

For the square graphite–epoxy plate described in section 3.2, we now investigate the increase in the buckling load caused by the bonding of 0.125 mm thick PZT-G1195 actuators to its top and bottom surfaces, cf figure 1. The PZT layers are poled in the X_3 direction. The attachment of the PZT layers to the graphite–epoxy plate will alter the buckling load. Nonzero values assigned to material parameters for the PZT-G1195 are listed below (see [22]):

$$c_1 = 29 \text{ GPa}, \qquad c_2 = 38.1 \text{ GPa}$$
$$c_3 = -2 \text{ GPa} \qquad c_4 = -21 \text{ GPa}$$
$$c_5 = 35.9 \text{ GPa} \qquad e_1 = 13.4757 \text{ C m}^{-2}$$
$$e_2 = -39.8583 \text{ C m}^{-2} \qquad \rho = 7500 \text{ kg m}^{-3}$$
$$\nu_4 = -90.3 \times 10^{-6} \text{ N V}^{-2} \qquad (15)$$
$$\nu_{12} = 30.54 \times 10^{-6} \text{ N V}^{-2}$$
$$\epsilon_0 = 8.8419 \times 10^{-12} \text{ N V}^{-2}$$
$$\epsilon_1 = 1.081 \times 10^{-9} \text{ N V}^{-2}$$
$$\epsilon_2 = -2.225\,58 \times 10^{-9} \text{ N V}^{-2}.$$

With these values of material parameters, constitutive relations (4) for the PZT contain second-order terms in the electric field $\boldsymbol{W}$ but only first-order terms in the Green–St Venant strain tensor $\boldsymbol{E}$. There is no test data available to find values of other material parameters. As shown in figure 1, uniformly distributed axial tractions are applied on the surfaces $X_1 = 0$, 10 mm of the graphite–epoxy plate. Because of the symmetry of the plate and the loading conditions about the centroidal axes of the plate that are parallel to the X_1 and X_2 axes, only a quarter of the plate was analyzed. The quarter of the graphite–epoxy plate was divided into uniform brick elements of size $0.5 \times 0.5 \times 0.042$ mm, and each one of the two PZT layers into uniform brick elements of size $0.5 \times 0.5 \times 0.125$ mm. A finer mesh could not be used because of the excessive CPU time required to reach the buckled state of the plate. A typical time step size used was 10^{-8} s and the plate buckled at $t \simeq 3 \times 10^{-4}$ s. The initial shape of the plate was assumed to be sinusoidal in both the X_1 and X_2 directions as described in section 3.2. For the loading rate of 1600 GN m^{-1} s^{-1} and no voltage applied to the PZTs, table 2

Table 2. Dependence upon the initial imperfection of the buckling load for the graphite–epoxy plate with PZT layers affixed to its top and bottom surfaces and loaded at the rate of 1600 GN m^{-1} s^{-1}.

$\dfrac{\text{Initial centroidal deflection}}{\text{Plate thickness}} \times 100$	Dynamic buckling load kN m^{-1}
0.33	403.6
0.66	387.6
1.0	377.8
1.33	360.6

lists the computed buckling load for the graphite/epoxy plate with the two PZT layers.

For the amplitude of the initial sinusoidal shape of the plate equal to 0.166% of the plate thickness, the plate buckled with the centroidal deflection in a direction opposite to that of the initial shape of the plate. In the results presented below, the amplitude of the initial sinusoidal shape of the plate was set at 0.33% of the plate thickness. We note that, within the buckled plate, the maximum principal strain and the maximum shear strain at any point were computed to be 7 and 11%, respectively. Thus a neo-Hookean material model for the plate should give acceptable results.

At the loading rate of 1600 GN m^{-1} s^{-1}, the inertial effects will play a significant role. Also, the CPU time required to determine the buckling load is less at such high loading rates since the time step size is determined by the time taken for an elastic wave to travel through the smallest element in the mesh. Since our goal is to establish the enhancement of the buckling load by using PZT actuators, the value of the loading rate will not affect much the percentage gain achieved by using PZT actuators.

When a uniform electric potential ϕ_a of 10, 20 and 30 V was applied only to the upper surface of the PZT layer bonded to the grounded top surface of the graphite–epoxy plate, the buckling load increased to 415.3, 456, and 403.8 kN m^{-1}, respectively. These represent an improvement of 2.95, 12.99 and 0.05% over that for the no actuation case. Figure 2 depicts the time history of the deflection of the centroid of the graphite–epoxy plate for the four cases studied. It is clear that, for $\phi_a = 20$ and 30 V, the centroid of the plate deflects in a direction opposite to that when $\phi_a = 0$ and 10 V. This exercise suggests that increasing the voltage difference applied to the two surfaces of the upper PZT layer does not necessarily increase the buckling load. Large electric fields applied across a PZT plate can either depole it or change the direction of polarization; these effects were not accounted for in our study.

In the preceding exercise, the upper PZT was actuated irrespective of the direction of the deflection of the centroid of the plate. An improvement in the buckling load can be attained by applying a voltage difference to either the upper PZT actuator or the lower one, depending upon which way the plate deflects. For positive deflection (downwards) of the centroid of the graphite–epoxy plate, an electric potential equal to $10^7 |u_c|$ V was applied to the top surface of the upper PZT, and for negative deflection of the centroid of the plate, an electric potential of $-10^7 |u_c|$ V was applied to the bottom surface of the lower PZT layer. The displacement, u_c, of the centroid of the graphite–epoxy plate is measured in mm. As should be evident from the results plotted in figure 3, the buckling load
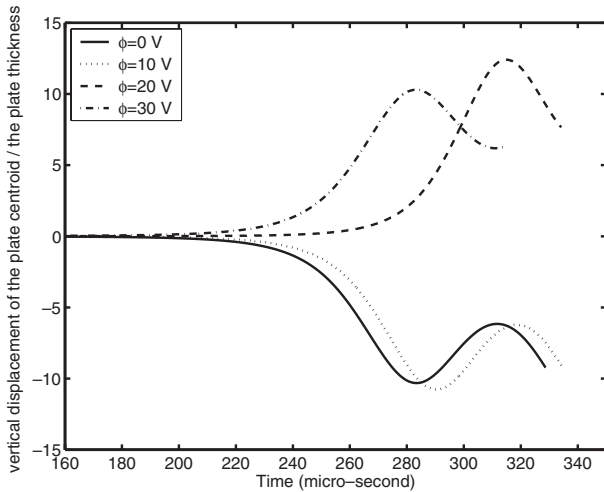
Figure 2. Time history of the deflection of the centroid of the axially loaded square graphite–epoxy plate when a voltage of 10, 20 and 30 V is applied to the upper surface of the PZT layer bonded to the top grounded surface of the plate.
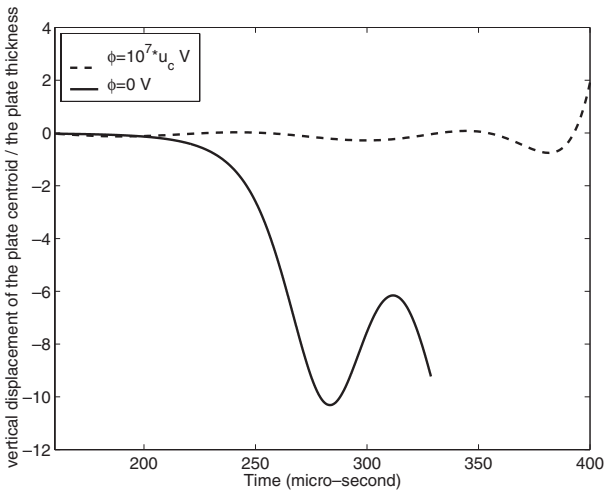

Figure 3. Time history of the deflection of the square graphite–epoxy plate's centroid when a voltage of $\pm 10^7 |u_c|$ is applied either to the bottom surface of the lower PZT layer or to the upper surface of the top PZT layer.

is considerably enhanced, and it equals 639.7 kN m^{-1}, which is 58.5% larger than that when PZT layers are not activated.

The 58.5% improvement in the buckling load resulted by applying a maximum electric field of 30 kV mm^{-1} which is quite large. We subsequently limited the maximum electric field to 1 kV mm^{-1}, and experimented with applying the electric fields at the rate of 10^6, 10^7 and $10^8 \times |u_c|$ V as stated above. For these three cases, the buckling load was found to increase by 1.14, 31.11 and 18.26%, respectively, suggesting that for the present problem, applying electric potential equal to $10^7 |u_c|$ V is the best option out of the three considered. In each case the plate deflected in the same direction.

A close study of the time history of the evolution of the centroidal deflection of the plate given in figure 2 reveals that our definition of the dynamic buckling load differs slightly from that of Budiansky and Hutchinson [16] and Cui *et al* [17]. Whereas the definition adopted herein determines the

Table 3. Dependence of the buckling load on values of material parameters ν_4 and ν_{12}.

Material parameters		Buckling load
$-10^5 \nu_4$	$-10^5 \nu_{12}$	kN m^{-1}
9.03	0	601
	0.0305	599
	3.05	529
	305	189
0	3.05	405
0.0903		334
9.03		529
903		407

buckling load uniquely, that of Budiansky and Hutchinson [16] corresponds to the load when the centroidal deflection begins to increase rapidly. The buckling load computed from Budiansky and Hutchinson's definition will be slightly smaller than that obtained with the present definition. Cui *et al* [17] equate buckling load to the point of intersection of the tangent to the rapidly rising part of the deflection versus load curve with the load axis. This will also give a smaller buckling load than that obtained with the present definition. Irrespective of the definition of the buckling load, the activation of the PZT layers will enhance the axial load at which the plate buckles.

In the constitutive relation (4) for a transversely isotropic PZT, there are eight terms with coefficients ν_2, ν_4, ν_7, ν_8, ν_{11}, ν_{12}, μ_1 and μ_2 that multiply quadratic terms in W. Because of a lack of test data to determine values of these parameters we had set six of them equal to zero. In table 3 we list the buckling loads for different values of the two nonzero parameters.

With all of the quadratic terms in W neglected in the constitutive relation (4), the buckling load equaled 322 kN m^{-1}. Thus the consideration of the two quadratic terms in the constitutive relation (5) generally enhances the dynamic buckling load, and the buckling load increases with a decrease in the magnitude of ν_{12}. However, the dependence of the buckling load on the values of ν_4 is not monotonic.

3.3.2. Effect of the size of the PZT actuators. Batra and Liang [23] found through numerical experiments the optimum location of a rectangular PZT actuator to annul different modes of vibration of a simply supported rectangular plate. The difference in the electric potential across the two faces of the PZT actuator is minimum if the centroid of the actuator is located at the point where the amplitude of vibration is maximum. Even though the plate does not necessarily undergo a steady vibratory motion in the present problem, we postulate that the PZT actuator is optimally located when its centroid coincides with the centroid of the plate. This is because the initial shape of the plate is assumed to vary sinusoidally in both X_1 and X_2 directions with the maximum deflection occurring at the center of the plate surface. Its buckled shape, exhibited in figure 4(*a*), closely resembles that of a plate vibrating in mode (1, 1). A comparison of the results plotted in figures 4(*b*) and (*c*) reveals that the rotations of the normals to the midsurface of the plate about the X_2 axis is more than that about the X_1 axis. It is most likely due to null tractions applied on the surfaces $X_2 = 0$ and 10 mm. The four different shapes
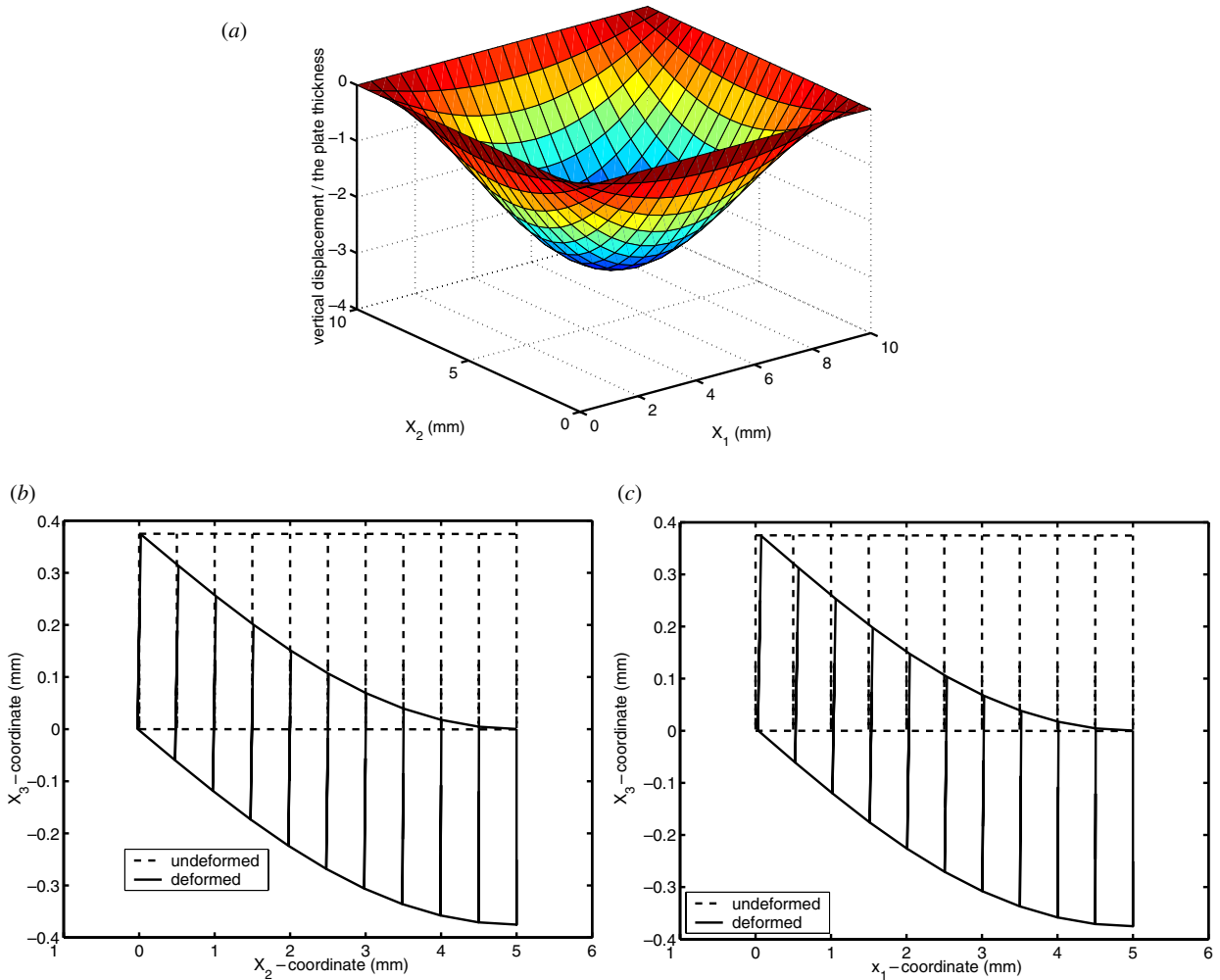
Figure 4. (*a*) The buckled shape of a square graphite–epoxy plate loaded on two opposite edges by uniformly distributed axial tractions that increase linearly with time, (*b*) view from the X_1-axis, (*c*) view from the X_2-axis.

of the PZT actuators, namely square, cross, rectangular fully extended in the X_1 direction, and rectangular fully extended in the X_2 direction, are shown in figure 5. The buckling load of the plate with the PZT patches bonded to its upper and lower surfaces will vary with the shape and the size of the patches. When used as actuators to enhance the buckling load, a voltage difference of $\max(10^7|u_c|, \ 125)$ V was applied across the two faces of the actuators. Figure 6 evinces the enhancement in the buckling load versus the fraction of the surface area of the plate covered by the PZT actuators for the four shapes delineated above. It is evident from these results that rectangular PZT patches fully extended in the X_2 direction are least effective in enhancing the dynamic buckling load. Also, cross-shaped and rectangular PZT patches fully extended in the X_1 direction are equally effective in increasing the buckling load during dynamic deformations of the plate. When the surface area of the plate covered by the PZT patches is at least 60%, the square PZT patches enhance the buckling load most. Recalling that the edge loads to the plate are applied in the X_1 direction, the computed results suggest that PZT patches extending along the direction of the load are quite effective in enhancing the buckling load of the plate.

3.3.3. Effect of the plate thickness relative to that of the PZT layers. For this study rectangular PZT layers fully extended in the X_1 direction and covering 90% of the surface area of the plate were considered. Keeping the thickness of each PZT layer fixed at 0.125 mm, the plate thickness was assigned the values 0.25, 0.75, 1.5, 2.25 and 3 mm. In each case, the quarter of the plate was divided into uniform $10 \times 10 \times 3$ elements, and the voltage applied to the PZTs equaled $\max(10^7|u_c|, \ 125)$ V. The corresponding enhancements in the buckling load were found to be 29.76, 15.21, 7.34, 0.71 and 0.31%, respectively. Thus an increase in the plate thickness relative to that of the PZT layers diminishes the effect of the PZTs in enhancing the buckling load.

3.3.4. Effect of the plate dimensions and boundary conditions. For $10 \times 10 \times 0.125$ mm, $50 \times 50 \times 0.625$ mm, $100 \times 100 \times 1.25$ mm, and $150 \times 150 \times 1.875$ mm substrate, the dynamic buckling load per unit edge length was found to be proportional to the length of a side of the plate, and the percentage gain in the dynamic buckling load caused by the PZT actuators remained unchanged. Also, the maximum principal strain and the maximum shear strain induced in each one of the four plates were the same.
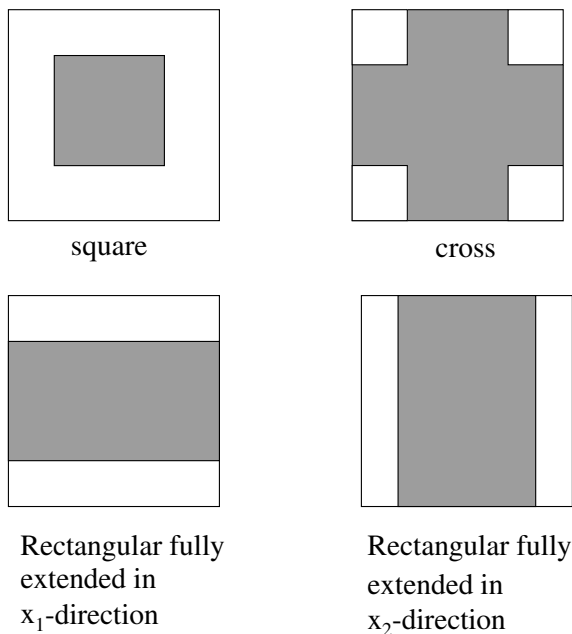
Figure 5. Four different shapes of PZT patches attached to the top and bottom surfaces of a square plate.
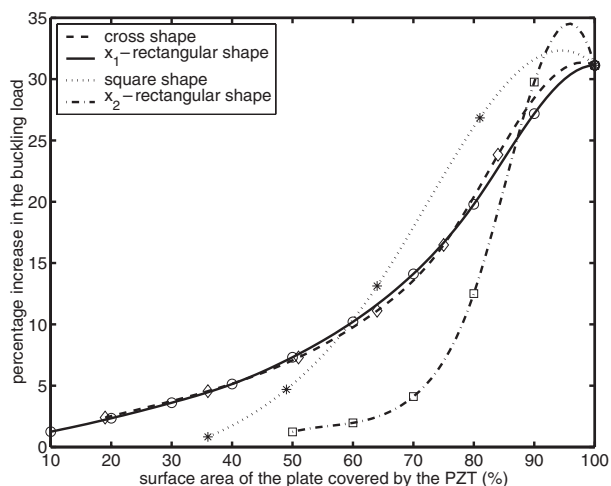

Figure 6. Enhancement in the buckling load of a square graphite–epoxy plate with PZT actuators bonded to its upper and lower surfaces versus the fraction of the surface area covered by the PZTs.

Figure 7 depicts the buckled shape of the plate when two opposite edges AE and BC are simply supported and the other two edges are traction free. It is clear that the deformed shape looks like a saddle rather than the double sinusoidal curve obtained when all four edges are simply supported.

4. Conclusions

We have used a three-dimensional geometrically nonlinear theory to investigate the enhancement in the dynamic buckling load of a graphite–epoxy square plate sandwiched between two piezoceramic layers. The simply supported plate is loaded on two opposite edges by equal and opposite in-plane compressive time-dependent tractions with the other
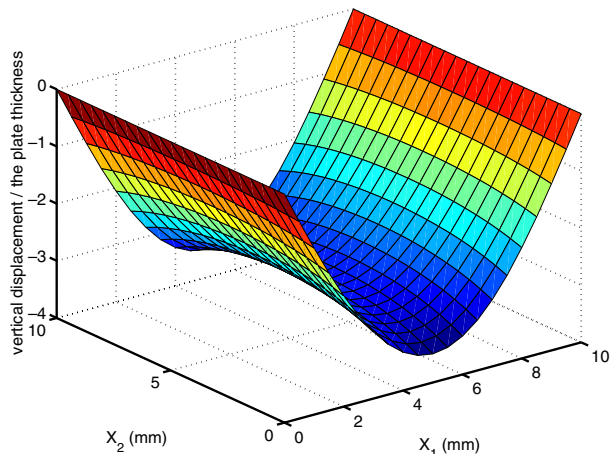

Figure 7. Buckled shape of the plate with two opposite edges simply supported and the other two edges traction free.

two edges kept traction-free. The plate material is modeled as neo-Hookean and the piezoceramic by a second-order constitutive relation, i.e. the second Piola–Kirchhoff stress tensor and the electric polarization are expressed as second degree polynomials in the Green–St Venant strain tensor and the electric field. The plate material is modeled as orthotropic and the PZT as transversely isotropic with the axis of transverse isotropy along the thickness direction. The transient problem is analyzed numerically by using the finite element code developed by Batra and Liang [3]. The plate is taken to have buckled when its centroidal deflection equaled three times the plate thickness.

The dynamic buckling load for the plate is found to strongly depend upon the rate of rise of the applied tractions and hence the inertia effects. With the maximum electric potential difference applied to the PZT layers limited to $1\,\text{kV}\,\text{mm}^{-1}$, the buckling load is enhanced by 18.3% when the PZT elements are activated. For a maximum electric field of $30\,\text{kV}\,\text{mm}^{-1}$, the buckling load increased by 58.5%. When only a part of the top and bottom surfaces of the plate can be covered by PZT layers, then square PZT elements provide a larger enhancement in the buckling load than rectangular shaped or cross-shaped PZT elements, provided that the covered surface area exceeds 60%. Otherwise the cross-shaped and rectangular PZT elements fully covering the square plate in the loading direction result in higher buckling loads than the square shaped PZT actuators.

An increase in the plate thickness relative to that of the PZT layers decreases the effectiveness of the PZTs in enhancing the buckling load for the plate. Of course, design considerations may limit the thickness of the PZT layers that can be used.

Even though we have not verified it, we believe that other definitions of the dynamic buckling load will not alter the qualitative nature of results but may change the magnitude of the gain in the buckling load achieved by activating the PZTs.

References

[1] Yang J S and Batra R C A second-order theory for piezoelectric materials *J. Acoust. Soc. Am.* **97** 280–8

[2] Crawley E F and Anderson E H 1990 Detailed models of piezoceramics actuation of beams *J. Intell. Mat. Struct.* **1** 4–24

[3] Batra R C and Liang X Q 1997 Finite dynamic deformations of smart structures *Comput. Mech.* **20** 427–38

[4] Chandrashekhara K and Bhatia K 1993 Active buckling control of smart composite plates—finite-element analysis *Smart Mater. Struct.* **2** 31–9

[5] Murali Krishna M W and Mei C 1992 Finite element buckling and post-buckling analysis of a plate with piezoelectric actuator *Proc. Conf. on Recent Advances in Adaptive Sensory Materials and their Applications (Blacksburg, VA)* (Blacksburg: Virginia Tech.) pp 301–13

[6] Thompson D M and Griffin O H Jr 1993 Finite element predictions of active buckling control of stiffened panels *J. Intell. Mater. Syst. Struct.* **4** 243–7

[7] Baz A and Tempe L 1989 Active control of buckling of flexible beams *Proc. ASME Design Technical Conf. (Canada, Montreal)* (New York: ASME) pp 211–8

[8] Thompson S P and Loughlan J 1995 The active buckling control of some composite column strips using piezoceramic actuators *Comput. Struct.* **32** 59–67

[9] de Faria A R and de Almeida S F M 1999 Enhancement of pre-buckling behavior of composite beams with geometric imperfections using piezoelectric actuators *Composites* B **30** 43–50

[10] Berlin A A and Sussman G J 1993 Increasing the compressive strength of a column via active control *Proc. Int. Conf. on Adaptive Structures* (Lancaster, PA: San Diego Technomic Publishing) pp 208–717

[11] Meressi T and Paden B 1993 Buckling control of a flexible beam using piezoelectric actuators *J. Guid. Control Dyn.* **16** 977–80

[12] Jefferis R P 1968 Feedback control of the buckling instability in an axially compressed thin elastic beam *PhD Thesis* Department of Electrical Engineering, University of Pennsylvania

[13] Berlin A A 1995 Active control of buckling using piezoceramic actuators *Industrial and Commercial Applications Smart Materials SPIE Smart Structures and Materials Workshop (San Diego, CA)*

[14] Berlin A A, Chase J G, Yim M, Maclean B J, Olivier M and Jacobsen S C 1988 MEMS-based control of structural dynamic instability *J. Intell. Mater. Syst. Struct.* **9** 574–86

[15] Petry D and Fahlbusch G 2000 Dynamic buckling of thin isotropic plates subjected to in-plane impact *Thin-Walled Struct.* **38** 267–83

[16] Budiansky B and Hutchinson J W 1964 Dynamic buckling of imperfection-sensitive structures *Proc. 11th Int. Congress of Applied Mechanics* (Berlin: Springer) pp 636–51

[17] Cui S, Hao H and Cheong H K 2001 Numerical analysis of dynamic buckling of rectangular plates subjected to intermediate-velocity impact *Int. J. Impact Eng.* **25** 147–67

[18] Batra R C 2000 Comparison of results from four linear constitutive relations in isotropic finite elasticity *Int. J. Nonlinear Mech.* **36** 29–40

[19] Batra R C and Yang J 1995 Second order constitutive relations for transversely isotropic porous piezoelectric materials *J. Acoust. Soc. Am.* **97** 2595–8

[20] Hughes T J R 1987 *The Finite Element Method, Linear Static and Dynamic Finite Element Analysis* (Englewood Cliffs, NJ: Prentice-Hall)

[21] Weller T, Abrmovich H and Yaffe R 1989 Dynamic buckling of beams and plates subjected to axial impact *Comput. Struct.* **32** 835–51

[22] Tiersten H F 1993 Electroelastic equations for electroded thin plates subjected to large driving voltages *J. Appl. Phys.* **74** 3389–93

[23] Batra R C and Liang X Q 1996 Shape control of vibrating simply supported rectangular plates *AIAA J.* **34** 116–22